Effects of $P_{\rm tot}$ gates and velocity gates on light-particle momentum correlation in intermediate-energy heavy-ion collisions

Ting-Ting Wang (王婷婷),[1,2,3] Yu-Gang Ma (马余刚),[1,2,3,*] and Zheng-Qiao Zhang (张正桥)[4,2]

[1]*Key Laboratory of Nuclear Physics and Ion-Beam Application (MOE), Institute of Modern Physics, Fudan University, Shanghai 200433, China*

[2]*Shanghai Institute of Applied Physics, Chinese Academy of Sciences, Shanghai 201800, China*

[3]*University of Chinese Academy of Sciences, Beijing 100049, China*

[4]*Shanghai Advanced Research Institute, Chinese Academy of Sciences, Shanghai 201210, China*

(Received 4 March 2019; revised manuscript received 29 April 2019; published 28 May 2019)

Momentum correlation functions at small relative momenta are calculated for light particles (n, p, d, t) emitted from ^{197}Au + ^{197}Au collisions at different impact parameters and beam energies within the framework of the isospin-dependent quantum molecular dynamics model complemented by the analytical method of Lednický and Lyuboshitz. We first make sure our model is able to reproduce the FOPI detector data of proton-proton momentum correlation in a wide energy range from 0.4A to 1.5A GeV. Then we explore more physics insights through the emission times and momentum correlations among different light particles. The specific emphasis is on the effects of total pair momentum among different light particles, impact parameters, and in-medium nucleon-nucleon cross sections. Both two-deuteron and two-triton correlation functions are anticorrelated due to the final state interaction, and they are affected by the in-medium nucleon-nucleon cross section for higher total momentum of the particle pairs, but not for lower momentum. In addition, impact parameter and in-medium nucleon-nucleon cross section dependences of the emission source radii are extracted by fitting the momentum correlation functions. The results indicate that momentum correlation function gating with total pair momentum is stronger for smaller in-medium nucleon-nucleon cross section factor (η) or impact parameter (b). Nonidentical particle correlations (np, pd, pt, and dt) are also investigated by velocity-gated correlation functions, which can give information on the particles' emission sequence, and the result indicates that heavier ones (deuteron and triton) are, on average, emitted earlier than protons, in the small relative momentum region.

DOI: 10.1103/PhysRevC.99.054626

I. INTRODUCTION

It is well known that the two-particle momentum correlation function at small relative momenta is sensitive to the space-time structure of particles at freeze-out, and therefore to the characteristics of the particle emission source [1–13]. At relativistic energy, the two-particle correlation function provides a very useful tool for measuring the freeze-out properties of partonic or hadronic systems [14–19] as well as interaction parameters between particle pairs [20–24]. In the intermediate-energy region, the two-proton correlation function has been used mostly as a probe of the space-time properties such as the source size and emission time in nuclear reactions [25–27]. The two-proton correlation function has been investigated in a lot of experiments and explored by different models, including various effects of the impact parameter [28,29], the total momentum of nucleon pairs [29], the isospin of the emission source [30], the nuclear symmetry energy [31], the nuclear equation of state (EOS) [29], and the in-medium nucleon-nucleon cross section (NNCS) [29,32], etc. Particularly, the dependence of the two-proton correlation function on the in-medium NNCS has been studied in more detail via Pratt's CRAB code [29] or using the code of Lednický and Lyuboshitz [32,33] in the framework of an isospin-dependent quantum molecular dynamics (IQMD) model. Since the magnitude of the total pair momentum is related to the nucleon emission time, the effect of total nucleon pair momentum on the strength of the correlation function was also discussed for heavy-ion collisions [29,31,34].

The correlation functions between two light charged particles other than two protons carry more information about the light particle production mechanism and reaction dynamics in heavy-ion collisions at intermediate energies [3,6,7,28,35–43]. In previous work [37,41,44,45], it was demonstrated that source sizes extracted from different particle species' correlation functions are different. This may be attributed to the dynamical expansion of the reaction zone and different timescales [46]. The simultaneous investigation of correlation functions involving composite light particles may offer a unique tool to investigate dynamical expansion of the reaction zone [7].

On the other hand, momentum correlations between two nonidentical particles contain information on the emission time differences of the two particles. Therefore, by comparing the correlation functions between two nonidentical particles

*Corresponding author: mayugang@cashq.ac.cn

with different velocity gates, one could infer the emission sequence between these two nonidentical particles [47–49], such as p, d, t, ^{3}He, and so on [8,49,50].

In this paper, we will discuss the correlation functions of light particles at different centralities and in-medium nucleon-nucleon cross section. In addition, we will investigate correlation functions of light particles under different total momentum of particle pairs. Furthermore, we also will check whether the strength of the correlation functions for light particle pairs with higher/lower total pair momenta is sensitive to the in-medium nucleon-nucleon cross section. On the other hand, for two nonidentical light particle pairs, we can get information about the order of emission time from their correlation functions gated with velocity selection. We have applied this method to the n-p, p-d, p-t, and d-t correlation functions for particles emitted in the lower relative momentum region.

To study the above questions quantitatively, a theoretical approach proposed by Lednický and Lyuboshitz [51] is applied for momentum correlation function construction based on the phase space data by an isospin-dependent quantum molecular dynamics (IQMD) model. To this end, we use the ^{197}Au + ^{197}Au system to investigate momentum correlation functions at different beam energies and impact parameters.

The rest of paper is organized as follows. In Sec. II, we briefly describe the Hanbury-Brown Twiss (HBT) technique using the Lednický-Lyuboshitz analytical formalism and an isospin-dependent quantum molecular dynamics model. In Sec. III, we show the results of the IQMD plus the Lednický-Lyuboshitz method for the study of proton-proton correlation function, where the results are compared with the FOPI detector experimental data. We then systematically discuss the light particle momentum correlation function and the influences of gates on the total momentum of the light particle pairs. A detailed analysis of light particle momentum correlation functions and extracted source size results is presented for different in-medium nucleon-nucleon cross sections and impact parameters for Au + Au collisions. Furthermore, correlation functions of nonidentical light particles are analyzed to deduce the emission time order of the two different particles in the lower relative momentum region. To conclude, Sec. IV gives a summary of the article.

II. FORMALISM AND MODELS

A. Lednický and Lyuboshitz analytical formalism

First, we present a brief review of a theoretical approach given by Lednický and Lyuboshitz [50–53] for the HBT technique and the understanding of physics in the present work. In such a framework, the main formula is based on the principle that the particle correlations when they are emitted at small relative momenta are determined by the space-time characteristics of the production processes owing to the effects of quantum statistics (QS) and final-state interactions (FSIs) [3]. Then, the correlation function can be expressed through a square of the symmetrizied Bethe-Salpeter amplitude averaging over the four coordinates of the emission particles and the total spin of the two-particle system, which represents the continuous spectrum of the two-particle state. In this model, the FSI of the particle pairs is assumed to be independent in the production process. According to the conditions in Refs. [48], the correlation function of two particles can be written as the expression

$$\mathbf{C}(\mathbf{k}^*) = \frac{\int \mathbf{S}(\mathbf{r}^*, \mathbf{k}^*)|\Psi_{\mathbf{k}^*}(\mathbf{r}^*)|^2 d^4\mathbf{r}^*}{\int \mathbf{S}(\mathbf{r}^*, \mathbf{k}^*) d^4\mathbf{r}^*}, \tag{1}$$

where $\mathbf{r}^* = \mathbf{x}_1 - \mathbf{x}_2$ is the relative distance of the two particles at their kinetic freeze-out, $\mathbf{k}^*$ is half of the relative momentum between two particles, $\mathbf{S}(\mathbf{r}^*, \mathbf{k}^*)$ is the probability of emitting a particle pair with given $\mathbf{r}^*$ and $\mathbf{k}^*$, i.e., the source emission function, and $\Psi_{\mathbf{k}^*}(\mathbf{r}^*)$ is the Bethe-Salpeter amplitude which can be approximated by the outer solution of the scattering problem [20]. In above limit, the asymptotic solution of the wave function of the two charged particles approximately takes the expression

$$\Psi_{\mathbf{k}^*}(\mathbf{r}^*) = e^{i\delta_c}\sqrt{A_c(\lambda)} \times \left[e^{-i\mathbf{k}^*\mathbf{r}^*}F(-i\lambda, 1, i\xi) + f_c(k^*)\frac{\tilde{G}(\rho, \lambda)}{r^*}\right]. \tag{2}$$

In the above equation, $\delta_c = \arg\Gamma(1 + i\lambda)$ is the Coulomb s-wave phase shift with $\lambda = (k^* a_c)^{-1}$, where a_c is the two-particle Bohr radius, $A_c(\lambda) = 2\pi\lambda[\exp(2\pi\lambda) - 1]^{-1}$ is the Coulomb penetration factor, and its positive (negative) value corresponds to repulsion (attraction). $\tilde{G}(\rho, \lambda) = \sqrt{A_c(\lambda)}[G_0(\rho, \lambda) + iF_0(\rho, \lambda)]$ is a combination of regular (F_0) and singular (G_0) s-wave Coulomb functions [52,53]. $F(-i\lambda, 1, i\xi) = 1 + (-i\lambda)(i\xi)/1!^2 + (-i\lambda)(-i\lambda + 1)(i\xi)^2/2!^2 + \cdots$ is the confluent hypergeometric function with $\xi = \mathbf{k}^*\mathbf{r}^* + \rho$, $\rho = k^* r^*$, and

$$f_c(k^*) = \left[K_c(k^*) - \frac{2}{a_c}h(\lambda) - ik^* A_c(\lambda)\right]^{-1} \tag{3}$$

is the s-wave scattering amplitude renormalized by the long-range Coulomb interaction, with $h(\lambda) = \lambda^2 \sum_{n=1}^{\infty}[n(n^2 + \lambda^2)]^{-1} - C - \ln[\lambda]$, where $C = 0.5772$ is the Euler constant. $K_c(k^*) = \frac{1}{f_0} + \frac{1}{2}d_0 k^{*2} + Pk^{*4} + \cdots$ is the effective range function, where d_0 is the effective radius of the strong interaction, f_0 is the scattering length and P is the shape parameter. The parameters of the effective range function are important parameters characterizing the essential properties of the FSI, and can be extracted from the correlation function measured experimentally [20,41,54]. Table I shows the parameters of the effective range function for different particle pairs in the present work.

In the above table, for n-n and n-p correlation functions, which include an uncharged particle, the Coulomb penetration factor $[A_c(\lambda)]$ is not considered and only the short-range particle interaction works. For charged particle correlation functions, only effect of the Coulomb interaction is expected to dominate the correlation functions of t-t, p-t, and d-t systems. However, excepting the Coulomb interaction, the short-range particle interaction dominated by the s-wave interaction is considered for p-p, d-d, and p-d particle pairs at small relative momenta. The correlation function of p-p particle pairs is dominated by only the singlet ($S = 0$) s-wave FSI

TABLE I. Experimental determination of the effective range function parameters for *n-n*, *p-p*, *t-t*, *p-d*, *p-t*, *d-t*, and *n-p* systems [20,41,54,55].

System	Spin	f_0 (fm)	d_0 (fm)	P (fm^3)
n-n	0	17	2.7	0.0
p-p	0	7.8	2.77	0.0
t-t	0	1×10^{-6}	0.0	0.0
p-d	1/2	−2.73	2.27	0.08
	3/2	−11.88	2.63	−0.54
p-t	0	1×10^{-6}	0.0	0.0
d-t	0	1×10^{-6}	0.0	0.0
n-p	0	23.7	2.7	0.0

contribution, while both spins 1/2 (*doublet*) and 3/2 (*quartet*) contribute in the case of the *p-d* system. However, for the deuteron-deuteron correlation function, a parametrization of the *s*-wave phase shifts δ has been used from the solution of $K_c(k^*) = \cot\delta$ for each total pair spin $S = 0, 1, 2$. Note that the effective range function for the total spin $S = 1$ is irrelevant, since it does not contribute due to the QS symmetrization.

B. The IQMD model

In a specific application of the Lednický-Lyuboshitz theoretical simulation, the true single-particle phase-space distribution at the freeze-out stage is required. In this paper, the isospin-dependent quantum molecular dynamics (IQMD) transport model is used as the event generator, which has been applied successfully to the HBT studies in intermediate-energy heavy-ion collisions (HICs) [29,32,35,56–59]. In the following discussion, we introduce the model briefly. The quantum molecular dynamics transport model is an *n*-body transport theory; it describes heavy-ion reaction dynamics from intermediate to relativistic energies [60–64]. Since the QMD transport model contains correlation effects for all orders, one can investigate various aspects of both the collision dynamics and the fragmentation process [32,59,65,66]. The main parts of QMD transport model address the following issues: the initialization of the projectile and the target, nucleon propagation under the effective potential, the collisions between the nucleons in the nuclear medium, the Pauli blocking effect, and the numerical tests.

The isospin-dependent quantum molecular dynamics transport model is based on the QMD transport model with the isospin factors. As we know, the main components of the dynamics in HICs at intermediate energies include the mean field, two-body collisions, and Pauli blocking. Therefore, it is important for these three components to include isospin degree of freedom in the IQMD transport model. What is more, due to a large difference between neutron and proton density distributions for nuclei far from the β-stability line, the samples of neutrons and protons in phase space should be treated separately in the projectile and target nuclei initialization.

In the IQMD model, the interaction potential is represented by the form

$$U = U_{\rm Sky} + U_{\rm Coul} + U_{\rm Yuk} + U_{\rm Sym} + U_{\rm MDI} + U_{\rm Pauli}, \quad (4)$$

TABLE II. The parameters of the interaction potentials.

α (MeV)	β (MeV)	γ	t_4 (MeV)	ε (MeV)	K (MeV)
−390.1	320.3	1.14	1.57	21.54	200
−129.2	59.4	2.09	1.57	21.54	380

where $U_{\rm Sky}$, $U_{\rm Coul}$, $U_{\rm Yuk}$, $U_{\rm Sym}$, $U_{\rm MDI}$, and $U_{\rm Pauli}$ are the density-dependent Skyrme potential, the Coulomb potential, the surface Yukawa potential, the isospin asymmetry potential, and the momentum-dependent interaction and the Pauli potential, respectively.

In particular, the density-dependent Skyrme potential $U_{\rm Sky}$ reads, when the momentum dependent potential is included,

$$U_{\rm Sky} = \alpha\left(\frac{\rho}{\rho_0}\right) + \beta\left(\frac{\rho}{\rho_0}\right)^{\gamma} + t_4 \ln^2\left[\varepsilon\left(\frac{\rho}{\rho_0}\right)^{2/3} + 1\right]\frac{\rho}{\rho_0}, \quad (5)$$

where ρ and ρ_0 are total nucleon density and its normal value, respectively. The parameters α, β, γ, t_4, and ε are related to the nuclear equation of state [67–70] and listed in Table II, where $K = 200$ or 380 MeV means the soft or the stiff momentum dependent potential, respectively.

A general review of the above potentials can be found in Ref. [60]. In the present work, the in-medium nucleon-nucleon cross section with isospin-dependence is represented by the formula

$$\sigma_{NN}^{\rm med} = \left(1 - \eta\frac{\rho}{\rho_0}\right)\sigma_{NN}^{\rm free}, \quad (6)$$

where ρ_0 is the normal nuclear matter density, ρ is the local density, η is the in-medium NNCS factor, and $\sigma_{NN}^{\rm free}$ is the available experimental NNCS [71]. The above reduction factor of the in-medium NNCS was introduced by the studies of collective flow in HICs at intermediate energies [72–74]. In particularly, the factor $\eta \approx 0.2$ has been found to better reproduce the flow data.

In this model, the particles are identified using a modified isospin-independent coalescence description, i.e., minimum spanning tree approach. In the minimum spanning tree approach, nucleons are assumed to share the same cluster if their centers are closer than a distance of 3.5 fm and their relative momentum is smaller than 0.3 GeV/c. In the present calculations, protons and neutrons are considered to be emitted when the surrounding density falls below a value of 0.02/fm^3 and there are unbound protons and neutrons, for which no other nucleon exists, within a coalescence distance of 3.5 fm and with relative momentum smaller than 0.3 GeV/c before the freeze-out time. If the nucleon is not bounded by any clusters, it is treated by an emitted (free) nucleon. In our calculations, the reactions of ^{197}Au + ^{197}Au are performed. We use the soft EOS with momentum dependent interaction for different impact parameters at different beam energies. For each run and particle species, the momentum correlation function is constructed when the system is basically at the

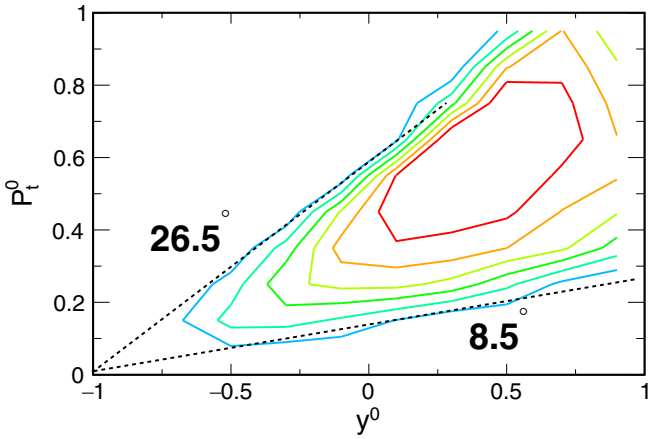

FIG. 1. Two-dimensional distribution of yields of proton in the P_t^0-y^0 plane for central ^{197}Au + ^{197}Au reactions. Target and projectile rapidities are given by $y^0 = -1$ and $+1$, respectively. The polar angle limits at 8.5 and 26.5 degrees.

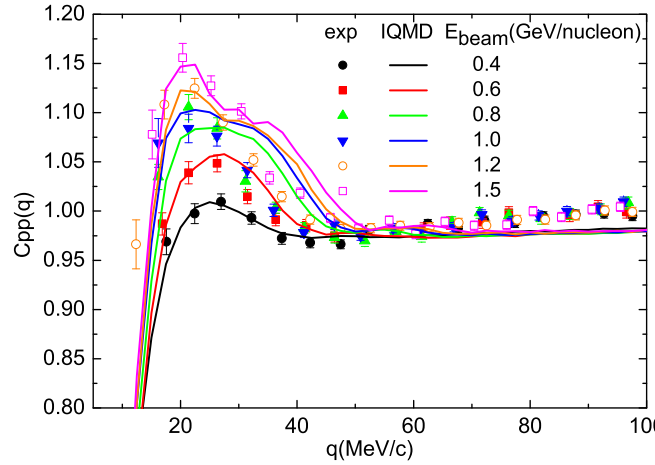

FIG. 2. Proton-proton correlation functions for the central Au + Au collisions at beam energies from 0.4A to 1.5A GeV. Experimental data (symbols) are compared to our predictions by the IQMD + FSI model calculation (lines).

corresponding freeze-out time and then processed within the Lednický-Lyuboshitz model.

III. ANALYSIS AND DISCUSSION

A. Comparison of the model predictions with experimental results

The collision centrality is an important variable for controlling reaction dynamics. Experimentally it could be estimated by the total multiplicity distribution of charged particles [8]. In previous FOPI experiments, total multiplicity distribution was measured in the outer Plastic Wall [8]. For a specific selection of central collision, the corresponding integrated cross sections for the collision system of Au + Au, about 10% of the total cross section has been selected [25]. To make a quantitative comparison with experimental data at 10% centrality [25], one would use the impact parameter of about 3 fm in the IQMD model for Au + Au collision, and the proton is selected in the polar angle $8.5^\circ \leqslant \theta_{\rm lab} \leqslant 26.5^\circ$, triggered in the middle rapidity as done in Ref. [25].

Figure 1 shows the phase space coverage corresponding to the experimental distributions in the c.m. system in central collisions. Here, $P_t^0 = (p_t/A_{\rm clus})/(p_{\rm proj}/A_{\rm proj})_{cm}$ and $y^0 = (y/y_{\rm proj})_{cm}$ are the normalized transverse momentum and rapidity, respectively. Within the above cuts of P_t^0 and y^0, we confront the experimental beam energy dependence of two-proton correlations with the predictions of the IQMD + Lednick-Lyuboshitz hybrid model. Figure 2 shows our calculated proton-proton correlation functions for central Au + Au collisions in comparison to the experimental results. In the figure, q at the x axis represents half of relative momentum of the particle pair, i.e., k^* in Eq. (1). In all following figures, q is the same quantity. With the above conditions in the transport approach, the correlation functions nicely agree with the data. We would like to point out that the fits of our correlation functions predicted by the IQMD to those from the experimental data are much better than those of previous correlation functions predicted by Boltzmann-Uehling-Uhlenbeck (BUU) calculations [25]. With increasing beam energy the peak of the proton-proton correlation function increases, and hence the apparent source radius decreases. The trend is similar to the one that can be found in Refs. [29,32].

B. Emission times of neutrons, protons, deuterons, and tritons

On the basis of the good fits of proton-proton momentum correlation between the data and our calculations, we will proceed in the following sections with more detailed calculations and discussion on momentum correlation functions among neutrons, protons, deuterons, and tritons, especially to investigate the effects of pair momentum cuts and the in-medium nucleon-nucleon cross section as well as the emission time sequence among neutrons, protons, deuterons, and tritons.

Here we are starting from the discussion of emission time distributions of different light particles since they are relevant for understanding both the collision dynamics and the mechanism of particle production. In heavy-ion collisions at intermediate energies, nucleon emissions are mainly governed by the pressure of excited nuclear matter during the initial stage of collision [34]. We performed calculations for different choices of a density dependent in-medium nucleon-nucleon cross section, with the η factors of 0.2 and 0.5 and impact parameter at $b = 0.0$ and 6.0 fm. In previous studies, the choice of $\eta = 0.2$ provides the best agreement with the balance energy in collective flow data. To see the η and impact parameter effects on light particle emissions, we show in Figs. 3(a)–3(d) the emission time distributions for neutrons, protons, deuterons, and tritons, respectively, for Au + Au collisions at 0.4A GeV. We can see that the emission time distribution of neutrons is similar to that of protons. However, the emission time distributions of light particles are different from those of protons and neutrons. While the proton and neutron emission time peaks earlier at about 50 fm/c, the emission time of light particles peaks later at about 60 fm/c. Regarding the η and impact parameter effects on particle emission, we find that the particle emission rates are larger

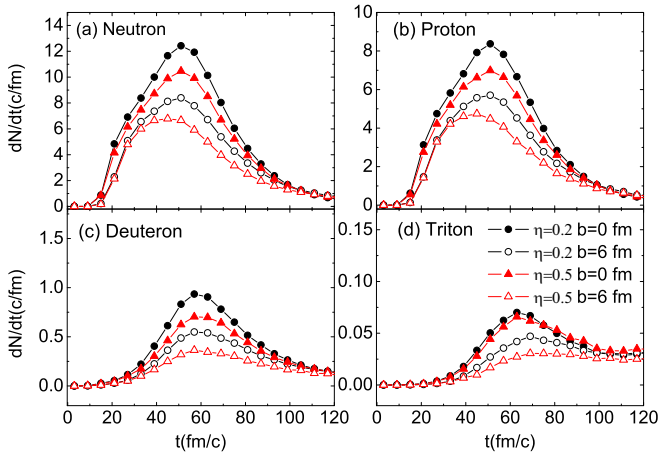

FIG. 3. Emission time distributions for neutrons (a), protons (b), deuterons (c), and tritons (d) for Au + Au collisions at 0.4A GeV with different in-medium nucleon-nucleon cross section factors ($\eta = 0.2, 0.5$) and impact parameters ($b = 0.0, 6.0$ fm).

in the cases of smaller η or b because the larger in-medium nucleon-nucleon cross section of central collisions gives a larger initial pressure which pushes more particle emission. For the emission time, there are only slight differences.

Particles emitted in an earlier stage of heavy-ion collisions usually have higher energy than those emitted during a later stage of the reaction. It is thus of interest to study the relationship between the average emission times of particles and their kinetic energy. Shown in Fig. 4 are the average emission times of neutrons, protons, deuterons, and tritons as a function of their c.m. kinetic energy under the same condition as in Fig. 3. We see that the particles with higher kinetic energies are emitted earlier than those with lower kinetic energies in central collisions (i.e., $b = 0$ fm). However, at $b = 6$ fm, the average emission times are not a monotonic function of the kinetic energy, especially for deuterons and tritons. The above difference indicates that there are different emission

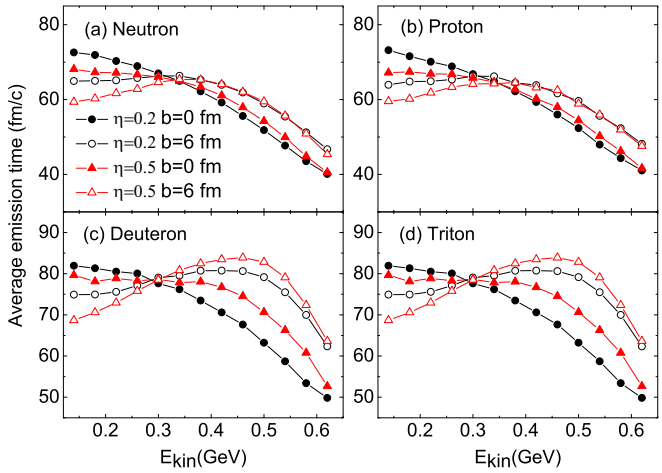

FIG. 4. Average emission times of neutrons (a), protons (b), deuterons (c), and tritons (d) as a function of their c.m. kinetic energy for Au + Au collisions at 0.4A GeV.

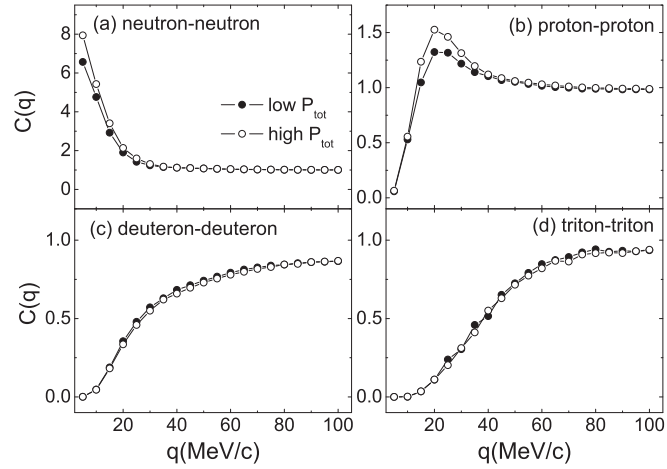

FIG. 5. Momentum correlation functions of particle pairs for Au + Au central collisions at 0.4A GeV with different cuts of total particle pair momentum. Open and filled circles correspond to high P_{tot} and low P_{tot} cuts, respectively. (a) Neutron pairs gated on P_{tot}: low, 0–0.4 GeV/c; high, 0.8–1.2 GeV/c. (b) Proton pairs gated on P_{tot}: low, 0–0.4 GeV/c; high, 0.8-1.2 GeV/c. (c) Deuteron pairs gated on P_{tot}: low, 0–0.8 GeV/c; high, 1.6–2.4 GeV/c. (d) Triton pairs gated on P_{tot}: low, 0–1 GeV/c; high, 2–3 GeV/c.

mechanisms in central collisions and semiperipheral collisions ($b = 6$ fm). In central collisions, most light particle emissions are mainly driven by a high-pressure dynamical source, but at semi-peripheral collisions light particle emissions are competed with by overlapping dynamical and thermal sources. In a higher relative kinetic energy region, e.g., above ∼0.32 GeV for neutrons and protons and 0.30 GeV for deuterons and tritons, the average emission times become later as η becomes larger, i.e., for smaller in-medium nucleon-nucleon cross section. However, in a lower relative kinetic energy region, the effect of in-medium nucleon-nucleon cross section on the average emission time is just the reverse.

C. Correlation functions of neutrons, protons, deuterons, and tritons

After discussing the emission times of neutrons, protons, deuterons, and tritons from Au + Au collisions at 0.4A GeV, we now proceed the systematical analysis of correlation functions for different particle pair combinations among neutrons, protons, deuterons, and tritons. The correlation functions will be discussed with specific gates on impact parameter, in-medium NNCS factor, total particle pair momentum, as well as the particle velocity. As mentioned in Sec. III A, our correlation functions are calculated by using the phase-space information from the freeze-out stage, which is used as the input for the Lednický-Lyuboshitz code, and then the effective source size is extracted by assuming a Gaussian-type emission source.

We first show in Fig. 5 four types of identical light-particle correlation functions, namely n-n, p-p, d-d, and t-t, for central collisions of ^{197}Au + ^{197}Au at $E = 0.4A$ GeV. The dependence of the strength of the correlation functions on total particle pair momentum (P_{tot}) will be discussed through

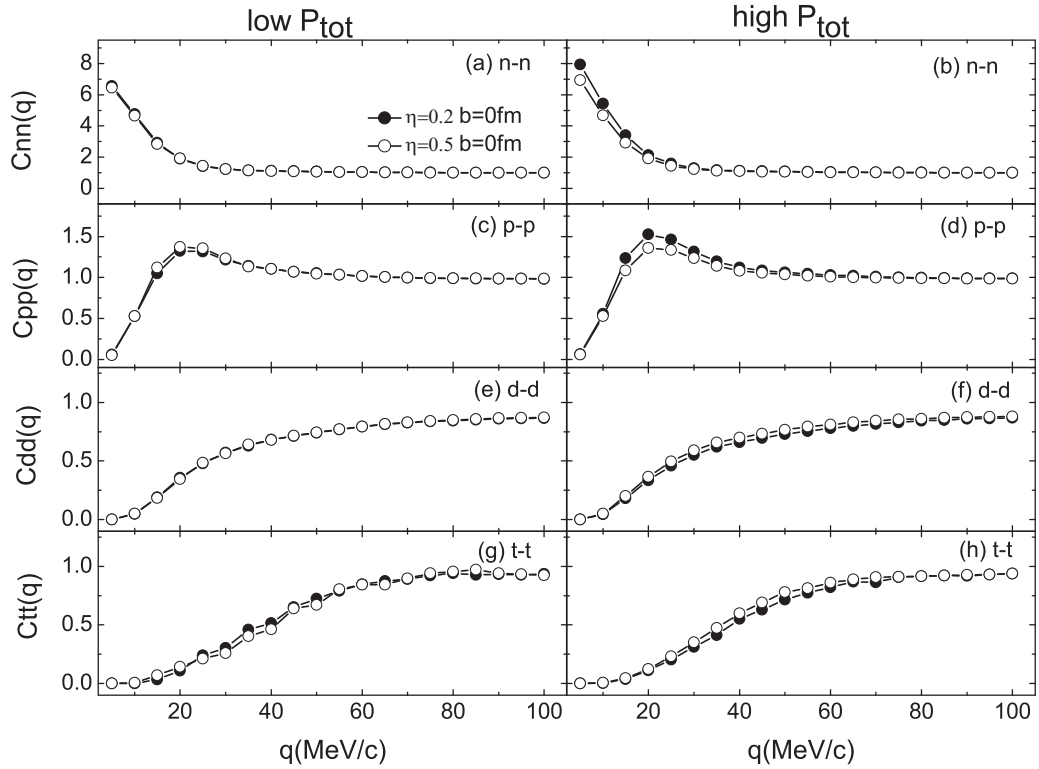

FIG. 6. Momentum correlation functions of particle-pairs as a function of different η factors in central collisions at incident energy $E = 0.4A$ GeV. Panels from top to bottom correspond to the correlation functions of neutron-neutron, proton-proton, deuteron-deuteron, and triton-triton pairs gated on low $P_{\rm tot}$ (left panels) and high $P_{\rm tot}$ (right panels), respectively.

calculations with two gates on $P_{\rm tot}$. In Fig. 5, the curves with open and filled circles are results with high $P_{\rm tot}$ and low $P_{\rm tot}$, respectively. Figures 5(a) and 5(b) show the two-neutron and two-proton correlation functions for two different total momentum ranges (low, 0–0.4 GeV/c; high, 0.8–1.2 GeV/c). The two-deuteron correlation function is presented in Fig. 5(c) gated on the different total momenta of deuteron pairs (low, 0–0.8 GeV/c; high, 1.6–2.4 GeV/c). Shown in Fig. 5(d) is the two-triton correlation function gated on different total momenta of triton pairs (low, 0–1 GeV/c; high: 2–3 GeV/c). From the figure, the shapes of the correlation functions are consistent with those observed in experimental data from heavy-ion collisions [75]. For the neutron-neutron correlation function, it peaks at $q \approx 0$ MeV/c. The two-proton (b), two-deuteron (c), and two-triton (d) correlation functions are all suppressed at low q because of Coulomb repulsion. The antisymmetrization of the two-proton wave function may also suppresses low-q pairs of protons, possibly enhancing this anticorrelation signal. With increasing relative momentum, for the two-proton correlation function, the strong final-state singlet-wave attraction gives rise to a maximum at $q \approx 20$ MeV/c. However, the two-deuteron correlation function does not exhibit a peak because of the anticorrelation between two-deuteron pairs induced by the repulsive singlet-wave nuclear potential and Coulomb potential. The two-triton correlation function is also anticorrelated as shown in Fig. 5(d) because only the Coulomb potential is included in the final-state interaction, as in Ref. [7]. In Figs. 5(a) and 5(b), it is clearly observed that the higher cut of $P_{\rm tot}$ leads to larger strength of the two-neutron and two-proton correlation functions. The trend implies that particles with higher momenta emitted earlier, or equivalently from a compact source, induce stronger correlation functions, consistent with the results shown in Fig. 4. The results are similar to those from a relatively simple approach in Refs. [76], which measured emission time for nucleons and light clusters in the coalescence model. The correlation between energy and emission time has been also clearly demonstrated in experimental data and model results for momentum-gated nucleon pairs, as demonstrated in Refs. [28,29,31,77]. The momentum correlation function is very complementary to above approach in terms of researching the properties and the space-time evolution of the reaction system. However, the sensitivity to total pair momentum becomes gradually weaker with increasing particle mass, e.g., for deuterons and tritons.

Next we will see the effect of in-medium nucleon-nucleon cross section on the momentum correlation function under different total pair momenta. In Fig. 6, the curves with filled and open circles are results with $\eta = 0.2$ and 0.5, respectively. They shows that the correlation functions of light particle pairs with high total momenta are more sensitive to the in-medium NNCS factor than those with low total momenta at the same impact parameter, since preequilibrium light particles with higher momenta are emitted earlier or have a smaller source size for smaller η. The η dependence of correlation functions with low total pair momenta shows opposite trend,

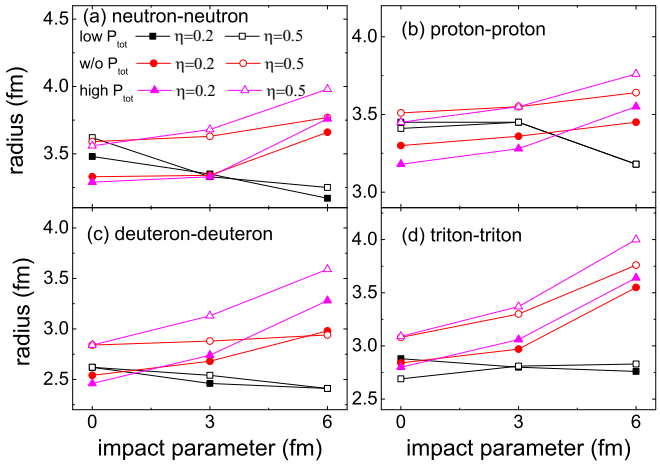

FIG. 7. Gaussian source radius as a function of impact parameter at different η factors at fixed incident energy 0.4A GeV. Panels (a) to (d) correspond to the Gaussian radius of neutron, proton, deuteron, and triton pairs, respectively.

and this is consistent with the η effect on particle emission times as shown in Fig. 4.

Figure 7 shows the dependence of radius extracted from light particle correlation functions on in-medium NNCS factor and impact parameter for different total pair momentum gates, where the squares and triangles are results with low $P_{\rm tot}$ and high $P_{\rm tot}$ cuts, respectively. The radii are extracted by a Gaussian source assumption, i.e., $S(\mathbf{r}^*) \approx \exp[-\mathbf{r}^{*2}/(4r_0^2)]$, where r_0 is the Gaussian source radius from the correlation functions. The results for light particle pairs without momentum gates are shown by the curve with circles, and are of course in between the results of the high $P_{\rm tot}$ and low $P_{\rm tot}$ cases. The extracted source radii from p-p (b) and n-n (a) are similar but quantitatively different, which might be due to the effect of Coulomb distortions in proton-proton pairs. Source radii from t-t (d) and d-d (c) correlation functions are generally smaller than those extracted from p-p (b) and n-n (a). For d-d and t-t correlations, as shown in Fig. 7, it is seen that the lower η, i.e., larger in-medium nucleon-nucleon cross section, leads to a slightly smaller radius, i.e., stronger anticorrelation of deuteron or triton pairs than those obtained with the larger η, particularly for deuteron or triton pairs with high $P_{\rm tot}$. For impact parameter dependence of the radii, we find that the radii in general increase with impact parameter except in the low $P_{\rm tot}$ case.

Finally, we also investigate the nonidentical particle correlation functions, such as p-d, p-t, d-t, and n-p. The p-d correlation function in Fig. 8(a) displays a single broad peak, due to both singlet-wave attraction and Coulomb repulsion. The shape is similar to the proton-proton correlation function while the peak is shown at about $q \approx 55$ MeV/c. However, the p-t and d-t correlation functions in Fig. 8(a) are characterized by an anticorrelation due to final-state Coulomb repulsion. Due to the s-wave attraction it peaks at $q \approx 0$ MeV/c for the neutron-proton correlation function. Except for the nonidentical particle correlation functions, the analysis of velocity-gated correlation functions of nonidentical particles is a very powerful tool to acquire detailed information about the particle emission time sequence [43,46–49,78,79]. Figure 8(b) shows the ratios of proton-deuteron, proton-triton, deuteron-triton, and neutron-proton correlation functions calculated with different velocity gates. The ratio is defined by comparing two velocity-gated correlation functions. The first function, $v+$ is constructed with pairs where the velocity of proton (deuteron) is faster than the deuteron (triton) or triton, respectively. The second function, $v-$ corresponds to the reverse situations. We obtain the emission sequences in nuclear collisions by a basic rule, as follows: if one of the two particles is emitted earlier and has lower velocity, it will, on average, travel a shorter distance before another particle is emitted. In our work, when the first emitted particle is slower than the second, the average distance will be reduced and the Coulomb suppression effect is thus enhanced, and vice versa. Therefore, in Fig. 8(b) a ratio of two different p-d and p-t correlation functions which is lower than unity indicates that deuterons

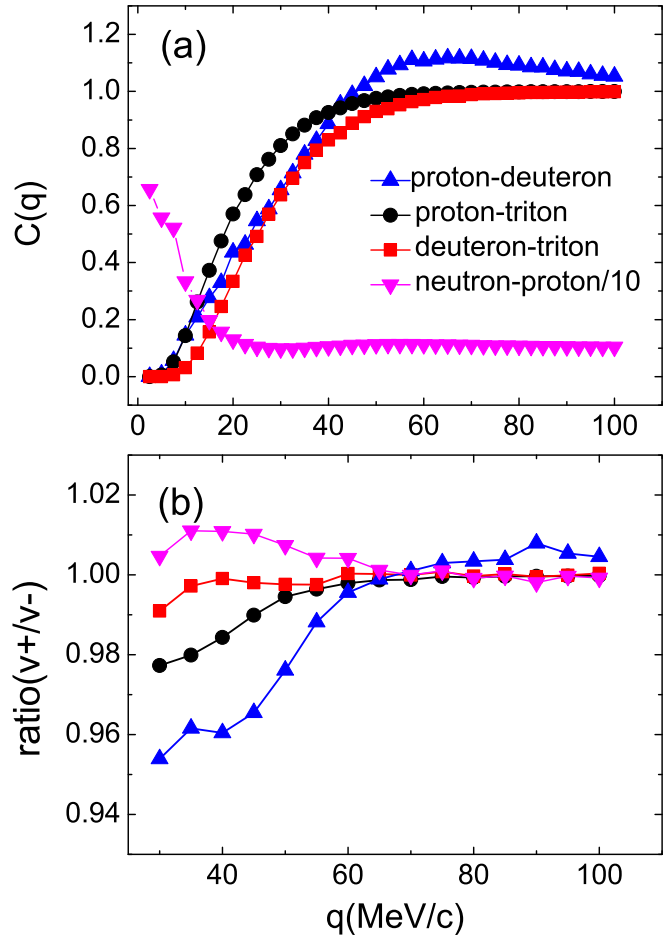

FIG. 8. Momentum correlation functions of nonidentical particle pairs for central Au + Au collisions at 0.4A GeV. The upper panel corresponds to proton-deuteron pairs, proton-triton pairs, deuteron-triton pairs, and neutron-proton pairs. The neutron-proton correlation function is scaled down 10 times. The bottom panel shows the ratio of both functions grouped into two velocity bins ($v+$ and $v-$), where $v+$ indicates that the first particle in a pair is faster than the second, and $v-$ is the reverse situation. See texts for details.

and tritons are, on average, emitted earlier than protons in the low relative momentum region. However, the ratios of n-p or d-t correlation functions are just slightly higher or lower than unity, respectively. The phenomenon indicates that the difference of emission time between neutron and proton or deuteron and triton is not so significant. It is consistent with the emission time in Fig. 3. In contrast, those particles are emitted on a similar timescale in the larger relative momentum region. The results are qualitatively consistent with other reaction systems: ^{36}Ar + ^{27}Al, ^{112}Sn, and ^{124}Sn at 61A MeV [80].

IV. SUMMARY

In summary, we present results of particle-particle momentum correlation functions reconstructed by the Lednický-Lyuboshitz analytical formalism using the phase-space points at the freeze-out stage for ^{197}Au + ^{197}Au collisions at different beam energies in a framework of the IQMD transport approach. As a necessary check of our model calculations, we performed a quantitative comparison of the proton-proton momentum correlation function with the FOPI data. Taking the same transverse momentum and rapidity phase space coverage corresponding to the experimental situation, it is found that with increasing beam energy from 0.4A to 1.5A GeV, the p-p correlation function becomes stronger, and our calculations can well reproduce the FOPI experimental data of the proton-proton correlation functions. After this essential verification os our model calculations, we can put forward for the following findings on emission time and momentum correlations of different light particles.

Emission time distributions of light particles and their dependence on particles' c.m. kinetic energy are studied by taking two different in-medium NNCS and impact parameter sets. We find that emission times are earlier for the particles with higher kinetic energies in central collisions. For semiperipheral collisions, the average emission times of deuterons and tritons first increase with the kinetic energy and then drop. At low kinetic energies, the larger in-medium nucleon-nucleon cross section makes the emission time longer; however, at higher kinetic energies, the effect is the reverse. It indicates that the different emission origins, i.e., the lower kinetic energy particles, are probably dominantly from statistical emission, while the higher ones are from preequilibrium dynamical process.

Momentum correlation functions with total momentum gated for all different pairs of particles containing neutrons, protons, deuterons, and tritons have been investigated. The two-particle correlation functions, especially for neutron-neutron and proton-proton pairs with higher total momentum are stronger than the one with lower total momentum. The correlation function of light particle pairs and the emission source size gated on higher total momentum are sensitive to impact parameter and in-medium NN cross sections: source size increases from central to semiperipheral collisions, and source size becomes larger in the larger η case, i.e., the smaller in-medium NN cross section.

Momentum correlation functions between nonidentical light particles can provide important information about the emission sequence and the radius of their emitting sources. The results indicate that heavier clusters (deuterons or tritons) are emitted earlier than lighter ones at same momentum per nucleon as expected from the analysis of velocity-gated correlation functions of nonidentical particles.

ACKNOWLEDGMENTS

This work is partially supported by the National Natural Science Foundation of China under Contracts No. 11890714 and No. 11421505, the Key Research Program of Frontier Sciences of the CAS under Grant No. QYZDJ-SSW-SLH002, and the Strategic Priority Research Program of the CAS under Grants No. XDPB09 and No. XDB16.

[1] G. I. Kopylov and M. I. Podgoredsky, Yad. Fiz. **18**, 656 (1973) [Sov. J. Nucl. Phys. **18**, 336 (1974)].
[2] G. I. Kopylov, Phys. Lett. B **50**, 472 (1974).
[3] S. E. Koonin, Phys. Lett. B **70**, 43 (1977).
[4] S. Pratt, Phys. Rev. Lett. **53**, 1219 (1984).
[5] S. Pratt, Phys. Rev. D **33**, 1314 (1986).
[6] S. Pratt and M. B. Tsang, Phys. Rev. C **36**, 2390 (1987).
[7] H. Boal, C. K. Gelbke, and B. K. Jennings, Rev. Mod. Phys. **62**, 553 (1990).
[8] R. Kotte *et al.*, Eur. Phys. J. A **6**, 185 (1999).
[9] N. A. Orr, Nucl. Phys. A **616**, 155 (1997); F. M. Marques *et al.*, Phys. Lett. B **476**, 219 (2000).
[10] W. G. Gong, W. Bauer, C. K. Gelbke *et al.*, Phys. Rev. Lett. **65**, 2114 (1990).
[11] J. Pochodzalla, C. B. Chitwood, D. J. Fields *et al.*, Phys. Lett. B **174**, 36 (1986).
[12] Y. G. Ma, D. Q. Fang, X. Y. Sun *et al.*, Phys. Lett. B **743**, 306 (2015).
[13] D. Q. Fang, Y. G. Ma, X. Y. Sun *et al.*, Phys. Rev. C **94**, 044621 (2016).
[14] M. A. Lisa, S. Pratt, R. Soltz, and U. Wiedemann, Annu. Rev. Nucl. Part. Sci. **55**, 357 (2005); M. A. Lisa *et al.*, Phys. Lett. B **489**, 287 (2000).
[15] J. Adams *et al.* (STAR Collaboration), Phys. Rev. Lett. **93**, 012301 (2004).
[16] A. Adare *et al.* (PHENIX Collaboration), Phys. Rev. C **92**, 034914 (2015).
[17] Z.-W. Lin, C. M. Ko, and S. Pal, Phys. Rev. Lett. **89**, 152301 (2002).
[18] J. Yang and W.-N. Zhang, Nucl. Sci. Tech. **27**, 147 (2016).
[19] H.-L. Lao, F.-H. Liu, B.-C. Li, and M.-Y. Duan, Nucl. Sci. Tech. **29**, 82 (2018).
[20] L. Adamczyk *et al.* (STAR Collaboration), Nature (London) **527**, 345 (2015).
[21] J. Adam *et al.* (STAR Collaboration), Phys. Lett. B **790**, 490 (2019).

[22] J. Adams *et al.* (STAR Collaboration), Phys. Rev. C **74**, 064906 (2006).
[23] L. Adamczyk *et al.* (STAR Collaboration), Phys. Rev. Lett. **114**, 022301 (2015).
[24] J. H. Chen, D. Keane, Y. G. Ma, A. H. Tang, and Z. B. Xu, Phys. Rep. **760**, 1 (2018).
[25] R. Kotte *et al.*, Eur. Phys. J. A **23**, 271 (2005).
[26] R. Ghetti *et al.*, Phys. Rev. Lett. **91**, 092701 (2003).
[27] D. Gourio *et al.*, Eur. Phys. J. A **7**, 245 (2000).
[28] W. G. Gong, W. Bauer, C. K. Gelbke, and S. Pratt, Phys. Rev. C **43**, 781 (1991).
[29] Y. G. Ma *et al.*, Phys. Rev. C **73**, 014604 (2006).
[30] R. Ghetti *et al.*, Phys. Rev. C **69**, 031605(R) (2004).
[31] L. W. Chen, V. Greco, C. M. Ko, and B. A. Li, Phys. Rev. Lett. **90**, 162701 (2003).
[32] T.-T. Wang, Y.-G. Ma, C.-J. Zhang, and Z.-Q. Zhang, Phys. Rev. C **97**, 034617 (2018).
[33] Y. X. Zhang, Z. X. Li, and P. Danielewicz, Phys. Rev. C **75**, 034615 (2007); B. Chen, F. Sammarruca, and C. A. Bertulani, *ibid.* **87**, 054616 (2013).
[34] L. W. Chen, C. M. Ko, and B. A. Li, Nucl. Phys. A **729**, 809 (2003).
[35] X. G. Cao, X. Z. Cai, Y. G. Ma, D. Q. Fang, G. Q. Zhang, W. Guo, J. G. Chen, and J. S. Wang, Phys. Rev. C **86**, 044620 (2012).
[36] C. B. Chitwood *et al.*, Phys. Rev. Lett. **54**, 302 (1985).
[37] J. Pochodzalla *et al.*, Phys. Rev. Lett. **55**, 177 (1985); Phys. Rev. C **35**, 1695 (1987).
[38] R. A. Kryger *et al.*, Phys. Rev. Lett. **65**, 2118 (1990).
[39] F. Zhu *et al.*, Phys. Rev. C **44**, R582 (1991).
[40] W. G. Gong *et al.*, Phys. Rev. C **47**, R429 (1993).
[41] B. Erazmus, L. Martin, R. Lednicky, and N. Carjan, Phys. Rev. C **49**, 349 (1994).
[42] T. M. Hamilton *et al.*, Phys. Rev. C **53**, 2273 (1996).
[43] G. Verde *et al.*, Eur. Phys. J. A **30**, 81 (2006); Phys. Lett. B **653**, 12 (2007).
[44] D. A. Cebra, W. Benenson, Y. Chen *et al.*, Phys. Lett. B **227**, 336 (1989).
[45] D. H. Boal and J. C. Shillcock, Phys. Rev. C **33**, 549 (1986).
[46] C. J. Gelderloos and J. M. Alexander, Nucl. Instrum. Methods A **349**, 618 (1994).
[47] C. J. Gelderloos *et al.*, Phys. Rev. Lett. **75**, 3082 (1995).
[48] R. Lednický, V. L. Lyuboshitz, B. Erazmus, and D. Nouais, Phys. Lett. B **373**, 30 (1996).
[49] S. Voloshin, R. Lednický, S. Panitkin, and N. Xu, Phys. Rev. Lett. **79**, 4766 (1997).
[50] R. Lednický and V. L. Lyuboshits, Sov. J. Nucl. Phys. **35**, 770 (1982).
[51] R. Lednický, Nucl. Phys. A **774**, 189 (2006).
[52] R. Lednický, Phys. Part. Nucl. **40**, 307 (2009).
[53] R. Lednický, Phys. At. Nucl. **71**, 1572 (2008).
[54] J. Arvieux, Nucl. Phys. A **221**, 253 (1974).
[55] L. D. Landau and E. M. Lifshitz, *Quantum Mechanics* (Nauka, Moscow, 1974).
[56] Y. G. Ma, X. Z. Cai, J. G. Chen *et al.*, Nucl. Phys. A **790**, 299c (2007).
[57] Y. B. Wei, Y. G. Ma, W. Q. Shen *et al.*, Phys. Lett. B **586**, 225 (2004).
[58] Y. B. Wei, Y. G. Ma, W. Q. Shen *et al.*, J. Phys. G **30**, 2019 (2004).
[59] T. T. Wang, M. Lv, Y. G. Ma *et al.*, Chin. Phys. Lett. **32**, 062501 (2015).
[60] J. Aichelin, A. Rosenhauer, G. Peilert, H. Stoecker, and W. Greiner, Phys. Rev. Lett. **58**, 1926 (1987).
[61] J. Aichelin, Phys. Rep. **202**, 233 (1991).
[62] G. Peilert, H. Stócker, W. Greiner, A. Rosenhauer, A. Bohnet, and J. Aichelin, Phys. Rev. C **39**, 1402 (1989).
[63] P.-C. Li, Y.-J. Wang, Q.-F. Li, and H.-F. Zhang, Nucl. Sci. Tech. **29**, 177 (2018).
[64] Z.-Q. Feng, Nucl. Sci. Tech. **29**, 40 (2018).
[65] C. W. Ma and Y. G. Ma, Prog. Part. Nucl. Phys. **99**, 120 (2018).
[66] T. Z. Yan, Y. G. Ma, X. Z. Cai *et al.*, Phys. Lett. B **638**, 50 (2006); T. Z. Yan and S. Li, Nucl. Sci. Tech. **30**, 43 (2019).
[67] B.-A. Li, L.-W. Chen, and C. M. Ko, Phys. Rep. **464**, 113 (2008).
[68] N.-B. Zhang and B.-A. Li, Nucl. Sci. Tech. **29**, 178 (2018).
[69] B.-J. Cai and L.-W. Chen, Nucl. Sci. Tech. **28**, 185 (2017).
[70] N.-B. Zhang, B.-J. Cai, B.-A. Li *et al.*, Nucl. Sci. Tech. **28**, 181 (2017).
[71] K. Chen *et al.*, Phys. Rev. **166**, 949 (1968).
[72] G. D. Westfall, W. Bauer, D. Craig *et al.*, Phys. Rev. Lett. **71**, 1986 (1993).
[73] D. Klakow, G. Welke, and W. Bauer, Phys. Rev. C **48**, 1982 (1993).
[74] Y. G. Ma and W. Q. Shen, Phys. Rev. C **51**, 710 (1995).
[75] R. Ghetti *et al.*, Nucl. Phys. A **674**, 277 (2000).
[76] K. Hagel, R. Wada, J. Cibor *et al.*, Phys. Rev. C **62**, 034607 (2000).
[77] N. Colonna *et al.*, Phys. Rev. Lett. **75**, 4190 (1995).
[78] C. J. Gelderloos *et al.*, Phys. Rev. C **52**, R2834 (1995).
[79] R. Ghetti *et al.*, Phys. Rev. Lett. **87**, 102701 (2001).
[80] R. Ghetti, J. Helgesson, and the CHIC Collaboration, Nucl. Phys. A **734**, 597 (2004).